High-Sensitivity Liquid Level Sensor Based on the Balloon-Shaped Fiber Optic MZI

Tutao Wang, Bo Liu, Lilong Zhao, Yaya Mao, Jianxin Ren, and Jiewen Zheng

***Abstract*—We demonstrated a high-sensitivity liquid level sensor based on the balloon-shaped fiber Mach-Zehnder interferometer (MZI). To make an optical fiber MZI sensor, a bare single mode fiber (SMF) is bent into a balloon shape. The sensor is attached to a stiff support and linked to a buoyancy ball floating on the liquid surface via a thin thread. The change in liquid level will bend the fiber and lead to a wavelength shift of transmission spectrum. This is a novel method of measuring liquid levels. We comprehensively studied the sensing performance of the sensor, and applied the ridge regression algorithm to optimize the fitting results of the experimental data. The maximum sensitivity of liquid level and temperature are 5.245 nm/mm and 40.3 pm/°C respectively, and the sensor has a low temperature cross-sensitivity of 0.00768 mm/°C. Furthermore, the sensor has the advantages of real-time response, convenient manufacture, low cost and high reliability, which broadens the application area of balloon-shaped MZI and makes it appropriate for liquid level sensing.**

***Index Terms*—Bent single mode fiber, fiber optic Mach-Zehnder interferometer, liquid level sensing, ridge regression.**

I. Introduction

In RECENT years, fiber optic sensors have attracted extensive attention because of their unique advantages such as small size, anti-electromagnetic interference, high sensitivity, and so on [1]–[3]. Fiber optic sensors have been used in the measurement of various physical quantities, such as liquid level [4], liquid salinity [5], high temperature [6], refractive index (RI) [7], etc. Among many physical quantities, liquid level measurement is critical in the special fields such as fuel storage, environmental monitoring and biochemistry. Optical fiber sensors have distinct advantages in liquid level sensing when compared with conventional electrical sensors, and there are no hidden dangers in measuring the level of flammable and explosive liquid. To date, many different types of fiber optic sensors for liquid level measurement have been proposed. For instance, based on the long-period fiber grating (LPFG) [8], fiber Bragg grating (FBG) [9]–[11], anti-resonance reflection guidance principle [12] and fiber modal interferometer [13] liquid level sensors came out one after another.

Ricchiuti *et al.* proposed a novel liquid level sensor with a measurement sensitivity of -12.71 dB/mm based on a 4cm LPFG [8]. Chang *et al.* proposed an ultra-sensitive liquid-level indicator using an etched chirped FBG with a sensitivity of 1.214 nm/mm, which can detect tens of micro-meter liquid-level variation [11]. By applying the Archimedes' law of buoyancy, Consales *et al.* present a simple and versatile fiber optic sensor for liquid level measurements based on the FBG [14]. In addition to the liquid level sensors with LPFG and FBG, the optical fiber interferometer-based liquid level sensors have attracted a lot of attention due to their advantages of compact structure, high reliability, and low fabrication cost. Among them, the liquid level sensor based on Fabry–Perot Interferometer (FPI) has been studied to a certain extent because of the advantage of non-direct contact with liquid measurement [15]–[17]. Jauregui-Vazquez *et al.* reported a liquid level fiber-optic sensor based on polymeric FPI with a sensitivity of 24.5 nm/m [16]. In addition, MZI and Michelson interferometer-based fiber optic level sensors have also been studied by many researchers. For example, Fabian *et al.* designed a multimode-coreless-multimode (MCM) fiber-optic structure for liquid level measurement [13]. Tian *et al.* used the dual side-hole fiber MZI to achieve high-sensitivity liquid level measurement and obtained a sensitivity of 4.019 nm/mm [18]. Wang *et al.* produced a highly sensitive liquid-level sensor based on an optical reflective microfiber probe and an ultra-high sensitivity of 367.644 nm/mm is achieved in experiment [19]. Based on the tapered PCF, Fan *et al.* designed a fiber optic MZI for measuring the liquid level and RI simultaneously. The liquid level and RI sensitivity are 0.58466 nm/mm and 195.969 nm/RIU [20], respectively. Sun *et al.* demonstrated a peanut-shaped optical fiber structure for liquid level sensing, and the sensitivity is only 0.1025 nm/mm [21]. However, the fiber optic liquid level sensors proposed so far are usually poor in sensitivity and complex to fabricate. At the same time, physical quantities such as the temperature and RI of the liquid will also cause a crosstalk to the liquid level measurement result. In addition, a small amount of liquid will adhere to the surface of the fiber when the liquid level varies in real-world applications, which will increase the response time of the sensor.

In this work, we proposed a high-sensitivity liquid level sensor based on the MZI sensor. The sensor is fabricated by bending the uncoated SMF into a balloon shape. A thin thread

Manuscript received December 21, 2021; revised February 16, 2022; accepted March 16, 2022. Date of publication March 28, 2022; date of current version April 6, 2022. This work was supported in part by the National Key Research and Development Program of China under Grants 2018YFB1800901 and 2018YFB1800905, in part by the National Natural Science Foundation of China under Grants 62075097, 62075038, 61975084, 61935005, 61835005, 61822507, 62005125, 61775098, 61875248, 61727817, U2001601, 62035018, 61720106015, and 61935011, in part by the Open Fund of IPOC, in part by the Jiangsu Talent of Innovation and Entrepreneurship, and in part by the Jiangsu Team of Innovation and Entrepreneurship. *(Corresponding author: Bo Liu.)*

The authors are with the Institute of Optics and Electronics, Nanjing University of Information Science and Technology, Nanjing 210044, China (e-mail: 1920765116@qq.com; bo@nuist.edu.cn; 001967@nuist.edu.cn; 002807@nuist.edu.cn; 003458@nuist.edu.cn; 403346219@qq.com).

Digital Object Identifier 10.1109/JPHOT.2022.3160735

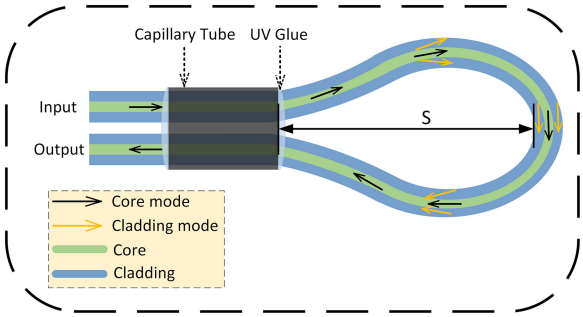

Fig. 1. The schematic diagram of the MZI sensor.

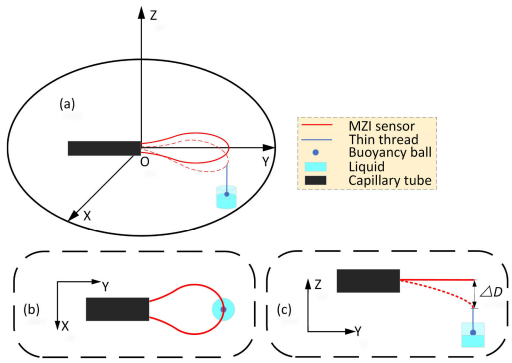

Fig. 2. The working schematic diagram of the optical fiber liquid level sensor.

connects the sensor to a buoyancy ball, which floats on the water owing to buoyancy. When the liquid level changes, the buoyancy ball exerts a drag force on the sensor through the thin thread, causing fiber bending and wavelength shift, resulting in a greater sensitivity than previously reported fiber liquid level sensors. Because the wavelength of transmission spectrum varies nonlinearly with the liquid level changes, we employ the ridge regression algorithm to fit the experimental data in order to produce a more accurate and reliable result. The results of the experimental reveal the maximum sensitivity of liquid level and temperature are 5.245 nm/mm and 40.3 pm/°C, respectively. The sensor has a low temperature cross-sensitivity (0.00768 mm/°C). Moreover, the sensor has the advantages of real-time response, convenient manufacture, low cost and high reliability. As such, we believe that the sensor we proposed will be conducive to the actual liquid level sensing.

II. Structure Design And Measurement Principle

The schematic diagram of MZI sensor is shown in Fig. 1. The manufacturing is a simple process that can be realized by using low-cost SMF. Firstly, the SMF with the coating layer removed is bent into the shape of a balloon, then the capillary tube is put on and the shape is fixed with ultraviolet (UV) glue, then turn into a finished sensor.

In Fig. 1, the distance between the top of the balloon-shaped fiber and the silicon tube is defined as S. When the light travels from the input port of the sensor to the bending part of the fiber, the conditions of total internal refraction can no longer be satisfied, and the partial light in the core will be excited into the higher-order cladding mode. When the light in the cladding travels through the total sensor, it will re-couple back to the core. During the whole transmission process, the inter-mode interference will occur due to the difference in the effective RI and optical path between the core and cladding modes. Thus, the intensity of the transmission spectrum can be written as [5], [22]:

$$I_{out} = I_{core} + I_{cladding} + 2\sqrt{I_{core} I_{cladding}} \cos\delta \quad (1)$$

where I_{core} and $I_{cladding}$ are the intensity of propagating in the fiber core and cladding respectively, and the phase difference between them is:

$$\delta = \frac{2\pi L_{eff} \Delta n_{eff}}{\lambda} \quad (2)$$

$$\Delta n_{eff} = n_{core}^{eff} - n_{cl,m}^{eff} \quad (3)$$

The value of δ will be affected as the change of liquid level, lead to a wavelength shift of transmission spectrum. Where λ and L_{eff} are the free-space wavelength and the effective interference length of the sensor, respectively. The effective RI difference between the fiber core and cladding modes is defined as Δn_{eff}. According to Eq. (1), it can be concluded that when δ is (2k+1) times π, interference dip appears in the transmission spectrum:

$$\frac{2\pi L_{eff}}{\lambda_k} \times (n_{core}^{eff} - n_{cl,m}^{eff}) = (2k+1)\pi, k = 0, 1, 2, 3 \ldots \quad (4)$$

thus, the interference dip wavelength λ_{dip} is given by:

$$\lambda_{dip} = \frac{2L_{eff}\Delta n_{eff}}{2k+1} \quad (5)$$

The working schematic illustration of the liquid level sensor is shown Fig. 2. In the coordinate system shown in Fig. 2(a). The silicon tube being arranged along Y-axis, and the two-dimensional plane formed by the balloon-shaped fiber is in the X-Y plane. The sensor and the buoyancy ball are connected by a thin thread. The top and front view of the Fig. 2(a) are shown in Fig. 2(b) and (c) respectively. As shown in Fig. 2(c), a change in liquid level causes the buoyancy ball to exert a drag force on the sensor through the thin thread, which can result in sensor deformation ΔD. The deformation of the optical fiber causes the MZI sensor's excitation and coupling point to move closer to the side of the silicon tube, which leads to the change of Δn_{eff} and L_{eff}. The wavelength shift of dip caused by the change in liquid level is:

$$\begin{aligned} \Delta\lambda_{dip} &= \frac{2(\Delta n_{eff} + \delta_n)(L_{eff} + \delta_l)}{2k+1} - \frac{2L_{eff}\Delta n_{eff}}{2k+1} \\ &= \frac{2\delta_l(\Delta n_{eff} + \delta_n) + 2\delta_n L_{eff}}{2k+1} \end{aligned} \quad (6)$$

where the δ_n and δ_l are the variation of Δn_{eff} and L_{eff} caused by the increased liquid level change, respectively. Thus, the dip of transmission spectrum appears a red shift as the increase of liquid level change. We can measure the change of liquid level by detecting the dip wavelength shift. According to Eq. (6), there is a linear relationship between the wavelength shift and liquid level change. However, when the liquid level changes too much, the

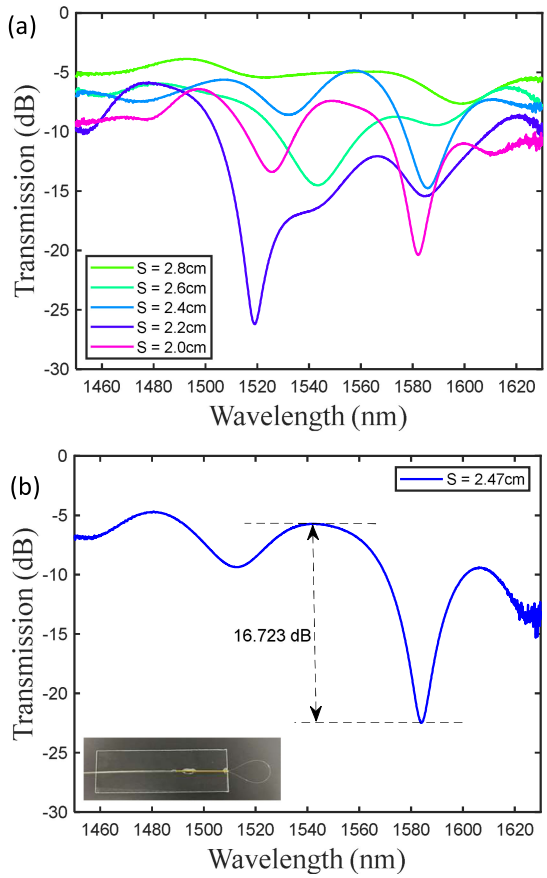

Fig. 3. (a) Transmission spectra of the balloon-shaped structure with different S; (b) Transmission spectrum when S is 2.47 cm.

wavelength shift will enter the nonlinear range. Consequently, we use the ridge regression algorithm to fit the experimental data to obtain a desired result. The loss function of ridge regression is given by:

$$J(\omega) = (X\omega - Y)^T(X\omega - Y) + \alpha\omega^T\omega \tag{7}$$

where ω is the regression factor, X and Y are the liquid level change and the wavelength of transmission spectrum respectively, $\alpha\omega^T\omega$ is the regular term. The optimal value of ω is obtained easily through the gradient descent algorithm:

$$\frac{\partial J(\omega)}{\partial(\omega)} = X^T X\omega - X^T Y + \alpha\omega \tag{8}$$

According to Eq. (5), S is the key parameter of the sensor. The value of S determines the size and bending degree of the MZI sensor, which will directly affect the value of Δn_{eff} and L_{eff}. The transmission spectra with different S are measured experimentally. As shown in Fig. 3(a), when S is equal to 2.8 cm, the interference dips begin to appear. With the decrease of S, interference dips become obvious and gradually increase. When S decreases from 2.8 to 2.0 cm, the extinction ratio of the interference spectrum increases first and then decreases. This is because that a lot of light travels to the cladding with the decrease of S, and the extinction ratio gradually increases. When S is small enough, too much light travels to the cladding and leaks

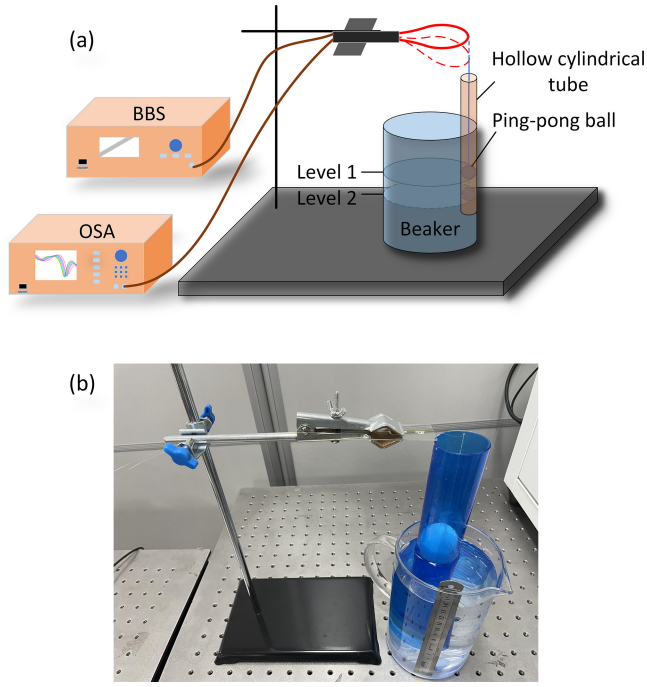

Fig. 4. (a) Diagram of liquid level sensing experimental device; (b) Physical image of the experimental device.

into the environment, resulting in the decrease of the extinction ratio. The smaller the S, the greater the bending degree of the balloon-shaped fiber, making the fiber more brittle. As a result, with a certain extinction ratio and insertion loss, S should be adjusted to a suitable value in order to preserve the structural stability of the sensor. S declines at 0.2 cm intervals rather than constantly in this work, implying that there may be an optimal S at varied lengths to obtain a superior overall performance. Considering the extinction ratio and structural stability of the transmission spectrum comprehensively, we finally adjusted the size of S to 2.47 cm. Currently, the extinction ratio of the transmission spectrum is 16.723 dB as shown in Fig. 3(b) and the structure is relatively stable. We will use this structure to subsequent sensing experiments.

III. Experimental and Results

The liquid level sensing characteristics of the sensor are studied in this paper. Fig. 4(a) illustrates the experimental liquid level sensing device. The light travels from the broadband light source (BBS) to the input port of the sensor, and the optical spectrum analyzer (OSA, YOKOGAWA, AQ6370D) receives and records the transmission spectra at various liquid levels. The sensor is fixed horizontally on the stiff support and connected to the buoyancy ball through a thin thread with a length of 12 cm. Fig. 4(b) shows the physical image of the experimental device. We use a ping-pong ball as the buoyancy ball due to the excellent buoyancy of itself. Meanwhile, the ping-pong ball will not only float up and down with the liquid level, but also float left and right on the surface of the water, which brings uncertainty to the experiment. In order to ensure that the ping-pong ball only floats up and down with the liquid level, we glue a hollow cylindrical

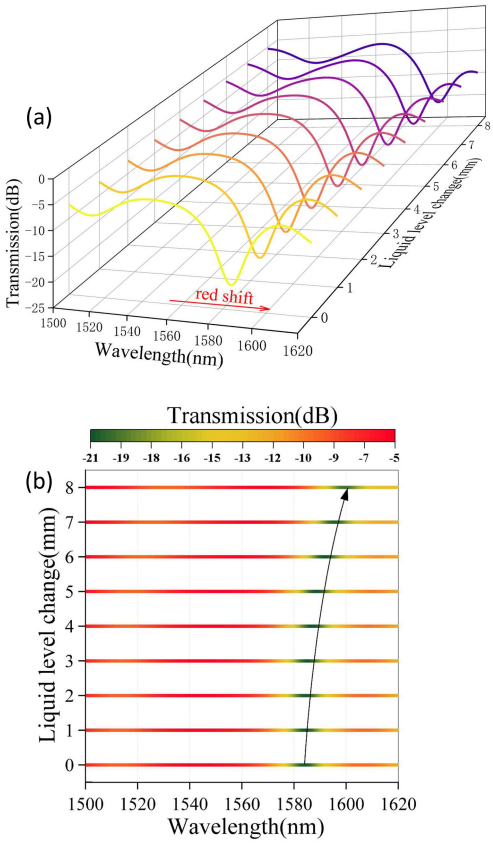

Fig. 5. The transmission spectra evolution with the liquid level change increases.

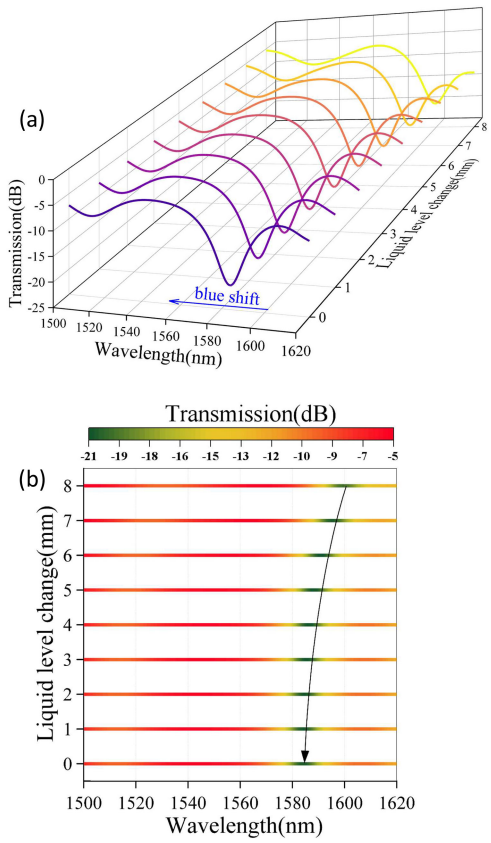

Fig. 6. The transmission spectra evolution with the liquid level change decreases.

tube vertically to the inside of the beaker and put the ping-pong ball into the tube. When the liquid level changes, the ping-pong ball will float along the tube in the vertical direction.

To study the liquid level response of the sensor, we first adjust the height of sensor and the position of ping-pong ball to make the thin thread vertical and relaxed. Then, to change the liquid level, we used a plastic dropper to draw water from the beaker at room temperature (about 20 °C), so the liquid level decreased and the change of the liquid level increased. The change of liquid level increased from 0 to 8 mm, and we used the OSA to record the transmission spectra for every 1mm increase as shown in Fig. 5(a) and (b). The dip of the transmission spectrum shifts to the side with a long wavelength (red shift). To test the repeatability of the sensor, we used the plastic dropper to drop water into the beaker to reduce the change of the liquid level from 8 to 0 mm. As shown in Fig. 6(a) and (b), we measured the transmission spectra for every 1mm decrease by the OSA. It can be found that the dip is moved in a direction opposite to the direction when the liquid level decreased, which moves to the side with a short wavelength (blue shift). The fitting result of the transmission spectra by using the ridge regression algorithm is shown in Fig. 7(a). The data in group1 and group2 show the dip shift with the liquid level change increases and decreases, respectively. The fitting results of the dip are non-linear, and the maximum sensing sensitivities is 4.445 nm/mm when the liquid level changed 8mm. It can be seen from Fig. 7(a) that the liquid level experiment result shows the excellent repeatability and consistency. In order to study the stability and response time of the liquid level sensor, the change of liquid level was firstly increased and then decreased, and the transmission spectra were recorded every ten seconds at each liquid level. As shown in Fig. 7(b), the dip wavelength depends on the liquid level variation in the time domain. The dip wavelength at the same liquid level remains within a slight error range. As the liquid level changes, the response is basically real-time, without obvious hysteresis. The results reveal the good stability and response speed in liquid level measurement of the proposed sensor.

Meanwhile, we conducted liquid level sensing experiment by changing the initial position of the ball. As shown in Fig. 8(a), the initial position of the ping-pong ball is placed in position 1 and position 2 respectively. At this time, the initial state of the thin thread is inclined. Fig. 8(b) is the top view of the sensor and ping-pong balls from above Fig. 8(a). As illustrated in Fig. 8(b), S1 and S2 are the distances of the ping-pong ball from the top of the sensor at position 1 and position 2 respectively, where both S1 and S2 are 1 cm. When the ping-pong ball at different positions, the fitting results are shown in Fig. 9(a) and (b). We got the maximum sensitivities of the sensor are 3.514 nm/mm and 5.245 nm/mm, respectively. As can be seen from the fitting results, there is slight difference between the three experiments. It means the initial position will impact the performance of sensor. Due to the stability is one of the most important parameters that

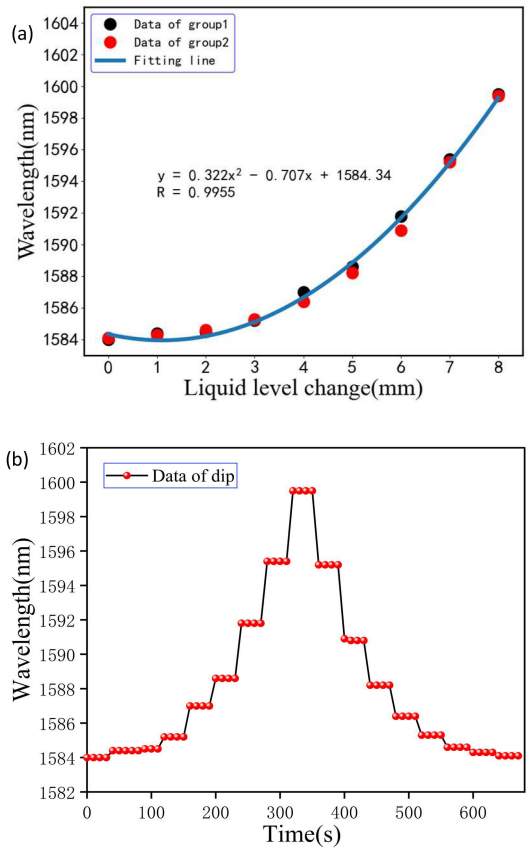

Fig. 7. Liquid level response of the sensor. (a) Data fitting of the dip; (b) The variation in the dip wavelength with liquid level in the time domain.

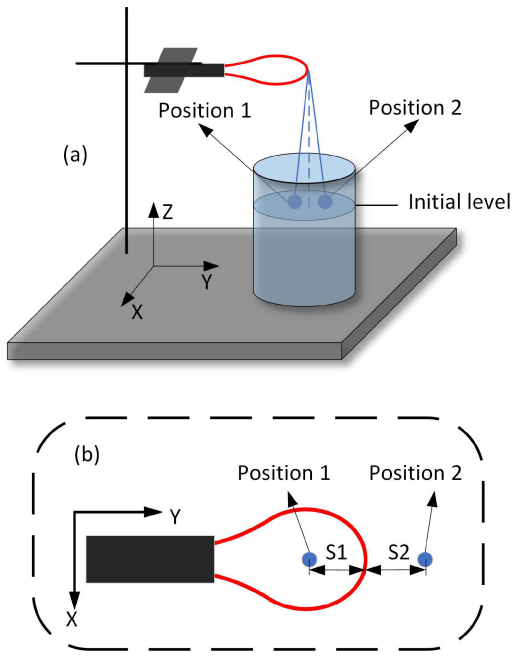

Fig. 8. (a) Schematic diagram of ping-pong ball at different positions; (b) The top view of the MZI sensor and ping-pong balls in Fig. 8(a).

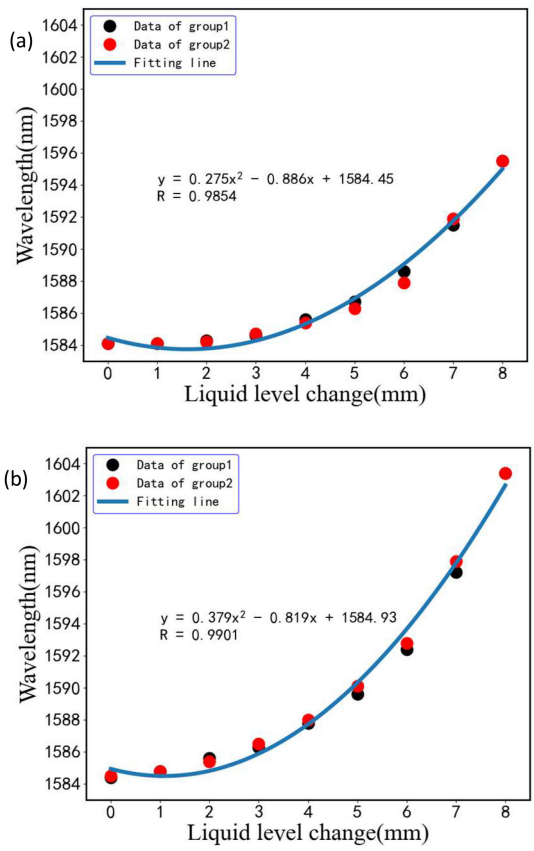

Fig. 9. (a) The fitting results of the ping-pong ball at position 1; (b) The fitting results of the ping-pong ball at position 2.

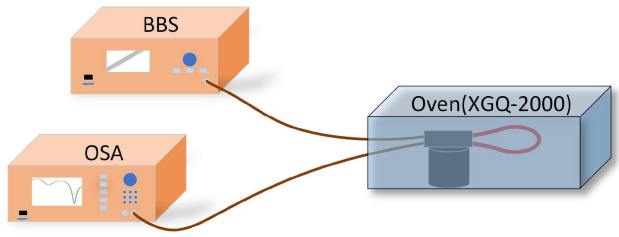

Fig. 10. Diagram of temperature sensing experimental device.

determine the overall measurement accuracy of a sensor, it is better to fix the initial position in real applications. But the liquid level sensing experiment exhibits a good repeatability and high fitting degree regardless the position of the ping-pong ball.

In addition, The MZI sensor is also sensitive to temperature due to the thermal expansion and thermal-optic effect of the optical fiber. As the temperature rises, L_{eff} and Δn_{eff} rise accordingly, resulting in a wavelength shift of dip:

$$\frac{\Delta\lambda_{dip}}{\lambda_{dip}} = (\alpha + \xi)\Delta T \tag{9}$$

where the α and ξ are the thermal expansion and the thermal-optic coefficients, respectively. ΔT is the amount of change in temperature. We can measure the ambient temperature change by detecting the wavelength shift of transmission spectrum. Fig. 10 depicts the diagram of temperature sensing experimental

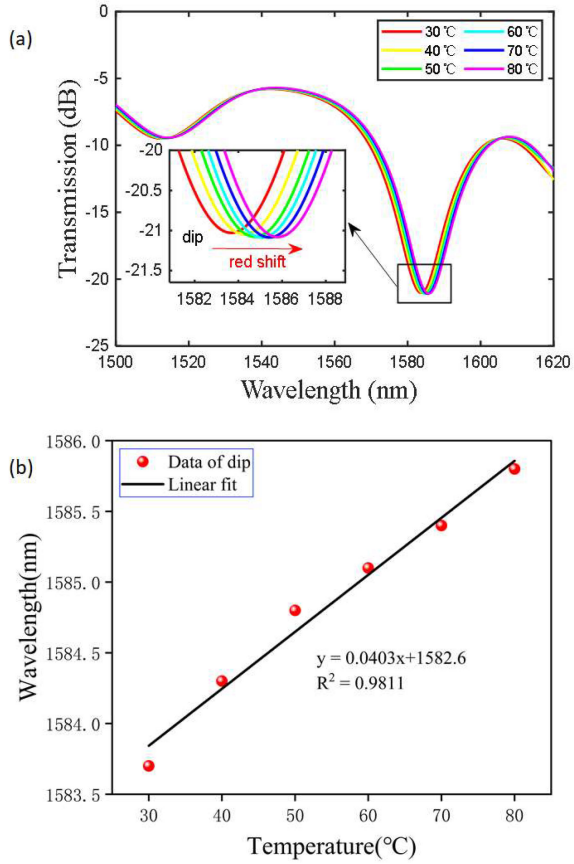

Fig. 11. (a) The transmission spectra evolution as temperature is changed; (b) Temperature response of the balloon-shaped MZI.

device. To conduct the temperature sensing experiment, we placed the sensor into the high-precision oven (XGQ-2000). The oven can accurately control the temperature with an error of ±1 °C. After travelling through the sensor, the light from BBS is received by OSA.

During the temperature sensing experiment, the temperature was raised from 30 to 80°C in 10°C increments by adjusting the high-precision oven. The transmission spectra were recorded for every 10 °C increase by the OSA. The transmission spectra at various temperature are shown in Fig. 11(a). As the temperature rises, the dip moves to the side with a long wavelength. Fig. 11(b) shows the fitting result of dip. The result exhibits a sensitivity of 40.3 pm/°C, with a highly linear response to temperature of 0.9811.

Through the liquid level and temperature sensing experiments, we can get the temperature cross-sensitivity of the sensor is 0.00768 mm/°C. Furthermore, when the wavelength resolution of OSA is 0.02 nm, the maximum liquid level and temperature resolutions are 0.0038 mm and 0.496 °C, respectively. This is acceptable in actual measurement. In the above sensing experiments, we use a wavelength demodulation scheme. Wavelength demodulation is the most common demodulation scheme in sensing systems and has a high universality. However, the sensing accuracy is limited, so it is necessary to use phase demodulation with higher demodulation accuracy in subsequent studies in order to improve the measurement accuracy [23].

TABLE I
COMPARISON OF SENSING PERFORMANCE OF DIFFERENT OPTICAL FIBER SENSORS

Sensor structure	Liquid level sensitivity (nm/mm)	Temperature sensitivity (pm/°C)	Indirect measurement	Temperature cross-sensitivity(mm/°C)	Ref.
Multimode fiber	0.41	36	No	0.0878	[3]
FBG	0.25 dB/mm	-42.4	No	0	[4]
LPFG	-12.71 dB/cm	-	No	-	[8]
Chirp FBG	1.214	8	No	0.0065	[11]
SMF-silica tube-SMF	0.4 dB/mm	16	No	0.004	[12]
MCM	0.73	-	No	-	[13]
FBG	0.0027	9	Yes	-	[14]
Vanadium doped fiber FPI	0.104	-	Yes	-	[15]
Polymeric FPI	0.0245	-	Yes	-	[16]
FBG and FPI	0.004	61.4	Yes	0	[17]
Dual side-hole fiber MZI	4.019	26.2	No	0.006	[18]
Microfiber-probe	367.644	-	No	-	[19]
Tapered PCF	0.585	8.97	No	0.01534	[20]
Peanut-shaped SMF	0.1025	38.7	No	0.37756	[21]
Balloon-shaped SMF	5.245	40.3	Yes	0.00768	This work

Table I compares the liquid level sensing performance of the sensor demonstrated in this paper with the other fiber optic sensors. Table I shows that the liquid level sensitivity of the sensor in this study is at a high level among all the sensors referenced. In addition to its high liquid level sensitivity, it also has the benefits of real-time reaction, being unaffected by the RI and temperature of the liquid, and so on. The sensor we presented is an excellent choice for liquid level sensing and shows the potential in the fiber optic liquid level sensing field.

IV. CONCLUSION

In summary, we introduced a liquid level sensor based on a balloon-shaped MZI sensor in this study. Liquid level sensing is accomplished by connecting the sensor with a ping-pong ball floating on the water surface through the thin thread, which improves the liquid level sensing sensitivity. The temperature and RI of the liquid have no bearing on the result of the liquid

level measurement. By adjusting the position of the ping-pong ball, the sensor achieves a maximum liquid level sensitivity of 5.245 nm/mm in the range of 0∼8 mm by applying the ridge regression algorithm. The temperature sensitivity is 40.3 pm /°C in the temperature range of 30∼80 °C, with a low temperature cross-sensitivity of 0.00768 mm/°C. The experimental results demonstrate the good repeatability and reliability in liquid level measurement of the sensor. Simultaneously, the sensor offers the advantages of real-time response, simple fabricate and low cost, making it appropriate for majority of practical liquid level sensing applications.

REFERENCES

[1] M. D. C. Alonso-Murias, J. S. Velazquez-Gonzalez, and D. Monzon-Hernandez, "SPR fiber tip sensor for the simultaneous measurement of refractive index, temperature, and level of a liquid," *J. Lightw. Technol.*, vol. 37, no. 18, pp. 4808–4814, 2019.

[2] N. F. Baharin, A. I. Azmi, A. S. Abdullah, and M. Y. Mohd Noor, "Refractive index sensor based on lateral-offset of coreless silica interferometer," *Opt. Laser Technol.*, vol. 99, pp. 396–401, 2018.

[3] O. Fuentes *et al.*, "Increasing the sensitivity of an optic level sensor with a wavelength and phase sensitive single-mode multimode single-mode fiber structure," *IEEE Sens. J.*, vol. 17, no. 17, pp. 5515–5522, Sep. 2017.

[4] R. Oliveira *et al.*, "Intensity liquid level sensor based on multimode interference and fiber Bragg grating," *Meas. Sci. Technol.*, vol. 27, no. 12, 2016, Art. no. 125104.

[5] T. Selokar and M. T. R. Giraldi, "All-fiber sensors for salinity and temperature simultaneous measurement," *Opt. Quant. Electron.*, vol. 53, no. 1, 2021.

[6] J. Mathew *et al.*, "In-fiber Fabry–Perot cavity sensor for high-temperature applications," *J. Lightw. Technol.*, vol. 33, no. 12, pp. 2419–2425, 2015.

[7] F. Chiavaioli, C. Trono, and F. Baldini, "Specially designed long period grating with internal geometric bending for enhanced refractive index sensitivity," *Appl. Phys. Lett.*, vol. 102, no. 23, 2013, Art. no. 231109.

[8] A. L. Ricchiuti *et al.*, "Continuous liquid-level sensor based on a long-period grating and microwave photonics filtering techniques," *IEEE Sens. J.*, vol. 16, no. 6, pp. 1652–1658, Mar. 2016.

[9] C. A. Marques, G. D. Peng, and D. J. Webb, "Highly sensitive liquid level monitoring system utilizing polymer fiber Bragg gratings," *Opt. Exp.*, vol. 23, no. 5, pp. 6058–6072, 2015.

[10] A. F. Obaton, G. Laffont, C. Wang, A. Allard, and P. Ferdinand, "Tilted fibre Bragg gratings and phase sensitive-optical low coherence interferometry for refractometry and liquid level sensing," *Sens. Actuators A, Phys.*, vol. 189, pp. 451–458, 2013.

[11] H.-Y. Chang *et al.*, "An ultra-sensitive liquid-level indicator based on an etched chirped-fiber Bragg grating," *IEEE Photon. Technol. Lett.*, vol. 28, no. 3, pp. 268–271, Feb. 2016.

[12] S. Liu, J. Tian, N. Liu, J. Xia, and P. Lu, "Temperature insensitive liquid level sensor based on antiresonant reflecting guidance in silica tube," *J. Lightw. Technol.*, vol. 34, no. 22, pp. 5239–5243, 2016.

[13] N. S. Fabian, A. B. Socorro-Leranoz, I. D. Villar, S. Diaz, and I. R. Matias, "Multimode-coreless-multimode fiber-based sensors: Theoretical and experimental study," *J. Lightw. Technol.*, vol. 37, no. 15, pp. 3844–3850, 2019.

[14] M. Consales *et al.*, "A fiber Bragg grating liquid level sensor based on the archimedes' law of buoyancy," *J. Lightw. Technol.*, vol. 36, no. 20, pp. 4936–4941, 2018.

[15] B. Preloznik, D. Gleich, and D. Donlagic, "All-fiber, thermo-optic liquid level sensor," *Opt. Exp.*, vol. 26, no. 18, pp. 23518–23533, 2018.

[16] D. Jauregui-Vazquez *et al.*, "Low-pressure and liquid level fiber-optic sensor based on polymeric Fabry-Perot cavity," *Opt. Quant. Electron.*, vol. 53, no. 5, 2021, Art. no. 237.

[17] J. Martins *et al.*, "Low-cost and high-performance optical fiber-based sensor for liquid level monitoring," *IEEE Sens. J.*, vol. 19, no. 13, pp. 4882–4888, Jul. 2019.

[18] Y. Tian *et al.*, "High sensitivity liquid level sensor based on dual side-hole fiber Mach–Zehnder interferometer," *Opt. Commun.*, vol. 440, pp. 194–200, 2019.

[19] J. Wang *et al.*, "Highly sensitive liquid-level sensor based on an optical reflective microfiber probe," *Opt. Lett.*, vol. 45, no. 1, pp. 169–172, 2019.

[20] R. Fan *et al.*, "Liquid level and refractive index double-parameter sensor based on tapered photonic crystal fiber," *J. Lightw. Technol.*, vol. 38, no. 14, pp. 3717–3722, 2020.

[21] M. Sun, Y. Jin, and X. Dong, "All-fiber Mach–Zehnder interferometer for liquid level measurement," *IEEE Sens. J.*, vol. 15, no. 7, pp. 3984–3988, Jul. 2015.

[22] S. K. Al-Hayali, A. M. Salman, and A. H. Al-Janabi, "High sensitivity balloon-like interferometric optical fiber humidity sensor based on tuning gold nanoparticles coating thickness," *Measurement,* vol. 170, 2021, Art. no. 108703.

[23] M. Galarza, R. A. Perez-Herrera, D. Leandro, A. Judez, and M. López-Amo, "Spatial-frequency multiplexing of high-sensitivity liquid level sensors based on multimode interference micro-fibers," *Sens. Actuators A, Phys.*, vol. 307, 2020, Art. no. 111985.